LES of a Spatially Developing Atmospheric Boundary Layer: Application of a Fringe Method for the Stratocumulus to Shallow Cumulus Cloud Transition

M. INOUE, G. MATHEOU, AND J. TEIXEIRA

Jet Propulsion Laboratory, California Institute of Technology, Pasadena, California

(Manuscript received 16 December 2013, in final form 9 April 2014)

ABSTRACT

An arrangement of a large-eddy simulation (LES) is described that facilitates a spatially developing thermally stratified atmospheric boundary layer (ABL). When the inflow and outflow boundary conditions are specified, the LES of stably stratified ABL turns out to be challenging because spurious reflections of waves at the boundary accumulate inside the domain. To tackle this problem, a fringe method with an auxiliary LES running concurrently is applied to enforce upstream/downstream boundary conditions. An artificial forcing term is applied within a fringe region located at the beginning of the main LES domain in order to ensure statistically stationary inflow boundary conditions. The auxiliary LES, which is horizontally homogeneous in a doubly periodic domain, is used to determine the inflow condition of the main LES domain. The present scheme is used to provide an Eulerian perspective of the stratocumulus to shallow cumulus cloud (Sc–Cu) transition, one of the key cloud regimes over the subtropical ocean. In this study, the transition is triggered by increasing the sea surface temperature (SST) and the LES runs until a statistically steady evolution of the Sc–Cu transition is achieved. The flow statistics are compared with those from a recycling-type method and it is found that the fringe method is more suitable for the current applications.

1. Introduction

Large-eddy simulation (LES) has been used to examine detailed turbulence processes in atmospheric boundary layers (ABLs). Our focus is a realistic LES of a spatially developing ABL, specifically an application to the stratocumulus to shallow cumulus cloud (Sc–Cu) transition, but the application of the method presented here is not restricted to this particular case. The Sc–Cu transition is one of the key cloud processes over the subtropical ocean and has been extensively studied over the past decade by LES (e.g., Krueger et al. 1995; Wyant et al. 1997; Bretherton et al. 1999; Sandu and Stevens 2011; Chung et al. 2012). Past LES investigations of not only the Sc–Cu transition but ABL in general have been often limited to cases where horizontally periodic boundary conditions are applied. Although it is advantageous to retain the periodicity that enables numerically accurate implementations, it potentially poses limitations on the modeling of spatially developing flows. A compromise in studies of the Sc–Cu transition is the quasi-Lagrangian analysis (e.g., Krueger et al. 1995; Stevens 2000; Sandu and Stevens 2011), where LES is forced by time-varying conditions that correspond to the mean advection of the whole ABL column inside the computational domain. A key disadvantage of the assumption that the entire column moves at constant horizontal velocity is that it does not allow the effect of differential advection with respect to height (De Szoeke and Bretherton 2004). Moreover, it has been shown that there are cases in which the temporal and spatial simulation of spatially developing flows may provide significantly different turbulent structures (see Schlatter et al. 2006).

Some authors (e.g., Mayor et al. 2002; Samelson et al. 2006; Skyllingstad et al. 2007; Nakayama et al. 2012) have conducted nonperiodic, spatially evolving LES of ABL by specifying inflow and outflow boundary conditions. The inflow boundary conditions are provided by the recycling method proposed by Lund et al. (1998). A recirculation region mimicking the periodicity is allocated in the upstream portion of the domain. Mayor et al. (2002) decomposed the inflow boundary conditions into a mean and a fluctuation. The mean of each variable is determined from precursor simulations and the fluctuation is copied from a downstream vertical plane. The

Corresponding author address: M. Inoue, Jet Propulsion Laboratory, California Institute of Technology, 4800 Oak Grove Dr., Pasadena, CA 91109.
E-mail: michio.inoue@jpl.nasa.gov

DOI: 10.1175/MWR-D-13-00400.1

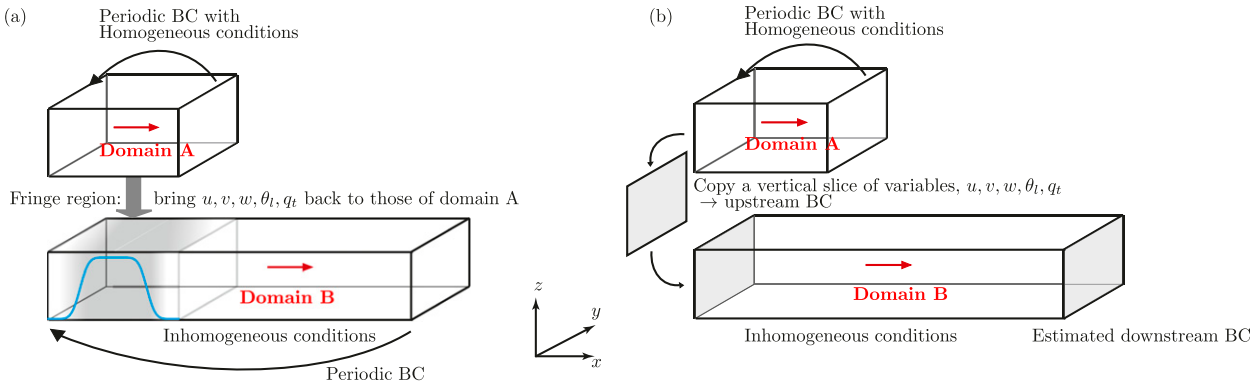

FIG. 1. A schematic view: (a) fringe method and (b) inflow–outflow method. A blue line within the fringe region shows the shape of the fringe function $\lambda(x)$.

inflow and outflow boundaries allow spatially developing simulations, but they have been somewhat limited in sampling time period or the domain depth. Mayor et al. (2002) hypothesized that this is because of the artificial reflection of gravity waves at the boundaries. One of the challenges in the stably stratified ABL application of this scheme is that it is difficult to damp or filter the undesired wave reflection. Designing the boundary condition, which allows flow to exit the computational domain without any artificial effects, remains an active research topic (e.g., Orlanski 1976; Klemp and Wilhelmson 1978; Davies 1983; Durran 1999; Colonius 2004).

An alternative is the fringe region technique that was first introduced by Spalart (1989) and has been employed in simulations of transitional turbulent boundary layers (e.g., Spalart and Watmuff 1993; Nordström et al. 1999). The flow crossing the downstream boundary is restored to the turbulence properties at the upstream boundary; hence, the computation domain keeps the horizontal periodicity. Despite this advantage, the fringe method has yet to be adapted and assessed for atmospheric flows. In this article, the fringe method is applied to LES of a spatially developing ABL, specifically the Sc–Cu transition. Although the focus is on the fringe method, a case is repeated using the inflow–outflow method to compare its performance in handling of the inhomogeneous boundary conditions.

2. Description of lateral boundary schemes

The goal is to facilitate a spatial evolution of the ABL triggered by spatially evolving climatological factors. Two schemes are described below (see Fig. 1). The schemes consist of two separate concurrently running LES: domains A and B. Domain A is an LES that is horizontally homogeneous with periodic lateral boundaries. Domain B is a spatially developing LES that is inhomogeneous in the streamwise direction and allows for spatially variable boundary conditions. Here the LES of domain A generates the field that is used to enforce the inflow boundary for domain B. Note that there is no feedback from domain B to A. The periodicity is enforced in the y direction. The treatment of the other lateral boundaries of domain B differs between the fringe and the inflow–outflow method.

a. The fringe method

The fringe region in domain B is indicated by the gray shading as shown in Fig. 1a. The ABL evolves along the x direction inside domain B and the flow is forced back to that of domain A within the fringe region. The region acts as a buffer for the flow leaving the domain and also for the upstream-propagating waves, so that the periodicity in the x direction can be enforced. This is realized by adding a linear damping term to the governing equations:

$$\frac{\partial \phi_B(x,y,z,t)}{\partial t} = N\phi_B(x,y,z,t) + \lambda(x)[\phi(x,y,z,t) - \phi_B(x,y,z,t)], \quad (1)$$

where N is the spatial operator of the Navier–Stokes equations, ϕ_B is a variable of domain B, and ϕ is the desired upstream condition. Originally, Nordström et al. (1999) damped the disturbances using a time-independent solution. However, the fringe method is typically robust enough to be able to set $\phi = \phi_A$, the instantaneous field of domain A. The fringe function $\lambda(x)$ is zero everywhere except at the beginning of the computational domain B. The region with nonzero $\lambda(x)$ is called the fringe region. Following Nordström et al. (1999), here we choose $\lambda(x)$ using the smooth function $S(x)$ as

$$\lambda(x) = \hat{\lambda}\left[S\left(\frac{x - x_{\text{start}}}{d_{\text{rise}}}\right) - S\left(\frac{x - x_{\text{end}}}{d_{\text{fall}}} + 1\right)\right], \quad (2)$$

where x_{start}, x_{end}, d_{rise}, and d_{fall} are design parameters that define the beginning, end, and shape of the fringe function, respectively, and

$$S(x) = \frac{1}{1 + \exp\left(\frac{1}{x-1} + \frac{1}{x}\right)}, \quad 0 < x < 1, \tag{3}$$

$S(x) = 0$ ($x \le 0$), and $S(x) = 1$ ($x \ge 1$). The sensitivity of the results to these parameters is out of scope of the current study and the parameters are set to a generic case with $\hat{\lambda} = 0.1$, $d_{\text{rise}} = d_{\text{end}} = L_{x,A}/2$, and $x_{\text{start}} = 0$, $x_{\text{end}} = L_{x,A}$, where $L_{x,A}$ is the length of domain A. The area of nonzero $\lambda(x)$ is equivalent to that of domain A.

b. *The inflow–outflow method*

The recycling method has been employed to provide the inflow boundary condition within one computational domain. However, to completely eliminate the effect of the downstream conditions that potentially propagates to the turbulent fluctuations upstream, the present method consists of two separate LES. Domain B uses inflow and outflow boundary conditions that replace the periodicity, thus the inflow–outflow method. The method is similar to that in Silva Lopes et al. (2007) and Chow and Street (2009) except that the two LES run concurrently. The variables on a vertical slice of domain A are used as the inflow boundary condition of domain B. At the end of the domain, in order to allow perturbations to pass out of the domain without any reflections, the Orlanski Doppler-shifted phase speed is employed here for the convective velocity u^*,

$$\frac{\partial u}{\partial t} + u^* \frac{\partial u}{\partial x} = 0, \quad \text{where} \quad u^* = \frac{\Delta x}{\Delta t} \frac{u^t_{b-1} - u^{t-1}_{b-1}}{u^{t-1}_{b-1} - u^{t-1}_{b-2}}, \tag{4}$$

where b represents the boundary grid index, t is the current time level, Δx is the grid spacing, and Δt is the time step (Mayor et al. 2002). When dealing with the incompressible or anelastic Navier–Stokes equations, it is necessary to adjust the solution of Eq. (4) to ensure the global mass conservation (Simens et al. 2009).

3. Large-eddy simulation

We demonstrate the performance of the two setups in simulating the Sc–Cu transition. Domain A generates a sheet of stratocumulus cloud with statistically steady properties that are used to enforce the inflow conditions of domain B. The Sc–Cu transition is triggered by spatially increasing SST along the streamwise direction. The LES implementation of Chung and Matheou (2014) and Matheou and Chung (2013, manuscript submitted to *J. Atmos. Sci.*) is used in the current simulations. Running the two LES simultaneously is achieved without any significant changes to the original code, by splitting a message passing interface (MPI) communicator into two nonoverlapping communicators.

Numerical details

The LES integrates the anelastic equations (Ogura and Phillips 1962). The base-state density $\rho_0(z)$ is calculated from the hydrostatic balance at constant base-state potential temperature $\Theta_{\text{ref}} = 300\,\text{K}$ and pressure $p_{\text{ref}} = 1000\,\text{hPa}$. The second-order energy-preserving advection scheme of Harlow and Welch (1965) is used for momentum advection to ensure that any dissipation arises purely from the SGS model. The advection scheme for the scalars is the second-order monotonized central-difference (MC) flux-limited scheme. Time is advanced using the low-storage, three-step Runge–Kutta of Spalart et al. (1991). The subgrid condensation is "all or nothing" (e.g., Cuijpers and Duynkerke 1993). The buoyancy-adjusted stretched-vortex subgrid-scale model (Misra and Pullin 1997; Voelkl and Pullin 2000; Pullin 2000; Chung and Matheou 2014) accounts for the unresolved turbulence physics with the additional subgrid-scale turbulence buoyancy production effect.

LES are initialized using the Atlantic Stratocumulus Transition Experiment (ASTEX) initial conditions (Duynkerke et al. 1999) and driven by SST-dependent Monin–Obukhov surface fluxes assuming full surface saturation at the local SST and surface pressure $p_{\text{srf}} = 1028.8\,\text{hPa}$. The entire domain is subject to the subsidence velocity $w_s = -Dz$, $D = 9.0 \times 10^{-6}\,\text{s}^{-1}$ and also to large-scale advection with a given height-independent horizontal gradient of Θ_l and total water mixing ratio Q_t, that are $\nabla_H \Theta_l = (0, 2.46 \times 10^{-6})\,\text{K m}^{-1}$ and $\nabla_H Q_t = (0, -1.96 \times 10^{-6})\,\text{g kg}^{-1}\,\text{m}^{-1}$, respectively. The Coriolis parameter is $f = 8.7 \times 10^{-5}\,\text{s}^{-1}$ and the height-independent geostrophic wind is $(u_g, v_g) = (3, 10)\,\text{m s}^{-1}$. A simplified radiation scheme, a sponge region near the top boundary, and other model-setup parameters follow that of Chung et al. (2012) to achieve statistically steady-state simulations.

The size of the domain A is $7.68\,\text{km} \times 5.12\,\text{km} \times 3.00\,\text{km}$ and the resolution is $\Delta_x = \Delta_y = 2\Delta_z = 80\,\text{m}$. The length of domain B is 15 times that of domain A (i.e., 115.2 km with the same grid resolution). The first 8 km of domain B have the same SST as domain A with constant SST = 294 K. SST then increases with a constant gradient, $2.0 \times 10^{-5}\,\text{K m}^{-1}$, until a 2 K of SST increase is achieved. See Fig. 2 for the SST profile within domain B. The flow field is first developed in domain A for 10 days until steady state is achieved and is subsequently copied to fill the entire domain B as 15 tiles of domain A. This minimizes the CPU time required to spin up the flow in

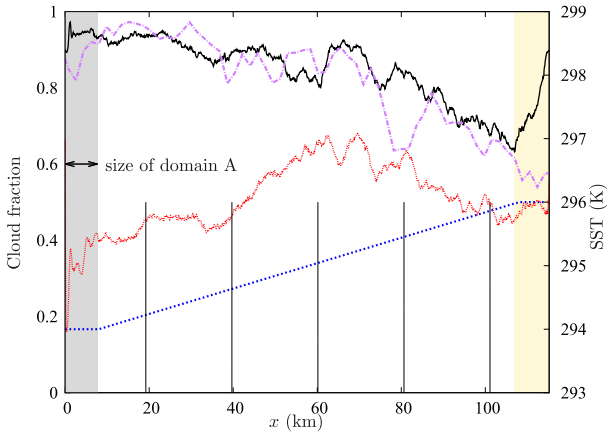

FIG. 2. Cloud fraction for the fringe method (black) and inflow–outflow method (red); and SST (blue) along the streamwise direction within domain B. SST increases from 294 to 296 K. The vertical lines indicate the locations where the vertical profiles are taken, specifically at $x = 19.20$, 39.68, 60.16, 80.64, and 101.12 km. The shaded areas indicate the regions contaminated by the fringe method: the fringe region (gray) and upstream effect of the fringe region (yellow); and a horizontally homogeneous LES (purple) where time was converted to distance by use of a mean advection speed (3.0 m s^{-1}).

domain B. The simulation is then continued for an additional 34 h until domain B reaches a statistically steady state. The statistics are averaged between 16 and 34 h with 10-min interval after the initialization using the fully developed flow field from domain A.

4. Results

Figure 2 compares the cloud fraction (CF), defined as the fraction of columns with liquid water mixing ratio $q_l > 10^{-5}$ kg kg^{-1} at any level. For the case of the fringe method, it demonstrates a continuous decrease in CF from close to 1 to about 0.6 toward the end of the domain. The linear forcing term inside the fringe region, indicated as a gray shade, successfully increases CF back to that of stratocumulus, although the increase begins upstream of the actual fringe region. Note that the fringe method uses the periodic boundary condition. The CF from a quasi-Lagrangian LES compares well with that of the fringe method, which verifies the results of the fringe method. The most significant difference between the two methods is at the beginning of the domain. Even with exactly the same inflow conditions (CF $\approx$ 1), the inflow–outflow method causes a sharp decrease of CF. It is observed that the decrease of the CF is amplified as time integration progresses.

Figure 3a visualizes the spanwise-averaged w and q_t at the beginning of domain B. It shows the gravity waves trapped at the inversion height that lead to the sharp

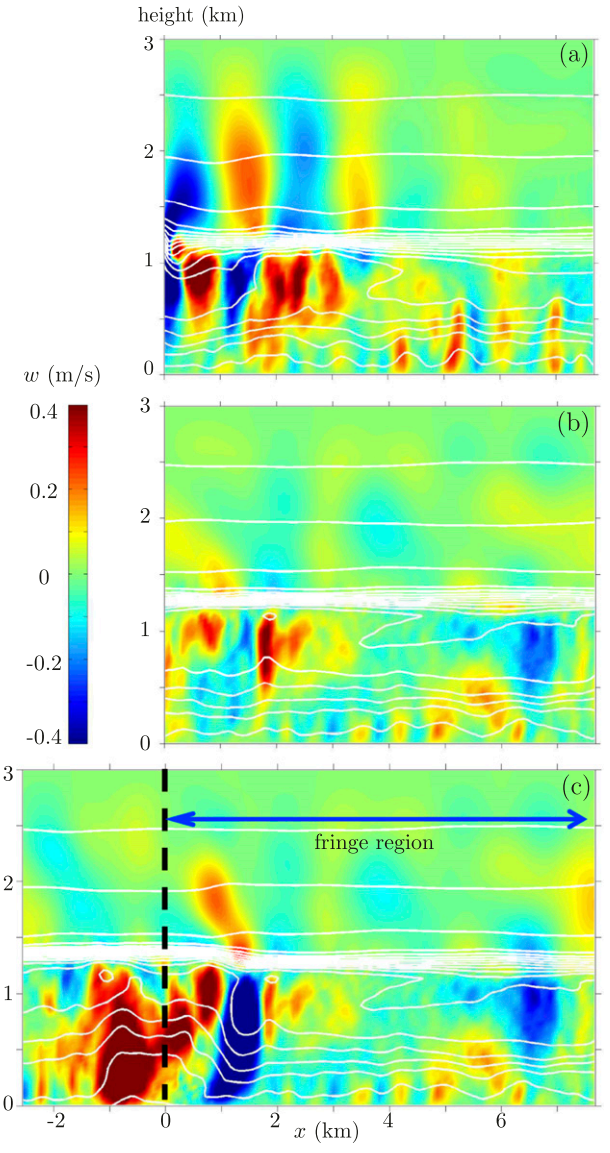

FIG. 3. Snapshots of the vertical velocity w (color) and the total water mixing ratio q_t [contours at 0.5 (g kg^{-1}) intervals]. Data are averaged over the y direction. (a) First $L_{x,A}$ of domain B from the inflow–outflow method, (b) domain A, and (c) first $L_{x,A}$ and last $L_{x,A}/3$ of domain B from the fringe method, where $L_{x,A}$ is the length of domain A. The fringe forcing is applied within the region indicated by the blue arrow.

decrease of CF and the dip in the height of the inversion within the first few kilometers. It is evident from Figs. 3b,c that the flow properties are forced back to those of domain A within the fringe region. Another pronounced feature is the strong positive vertical velocity close to the fringe region ($x \approx -1$ in Fig. 3c). As a result, larger total water mixing ratio and lower potential temperature at the lower ABL are convected upward, and produce more liquid water, which causes the increase of CF. It indicates

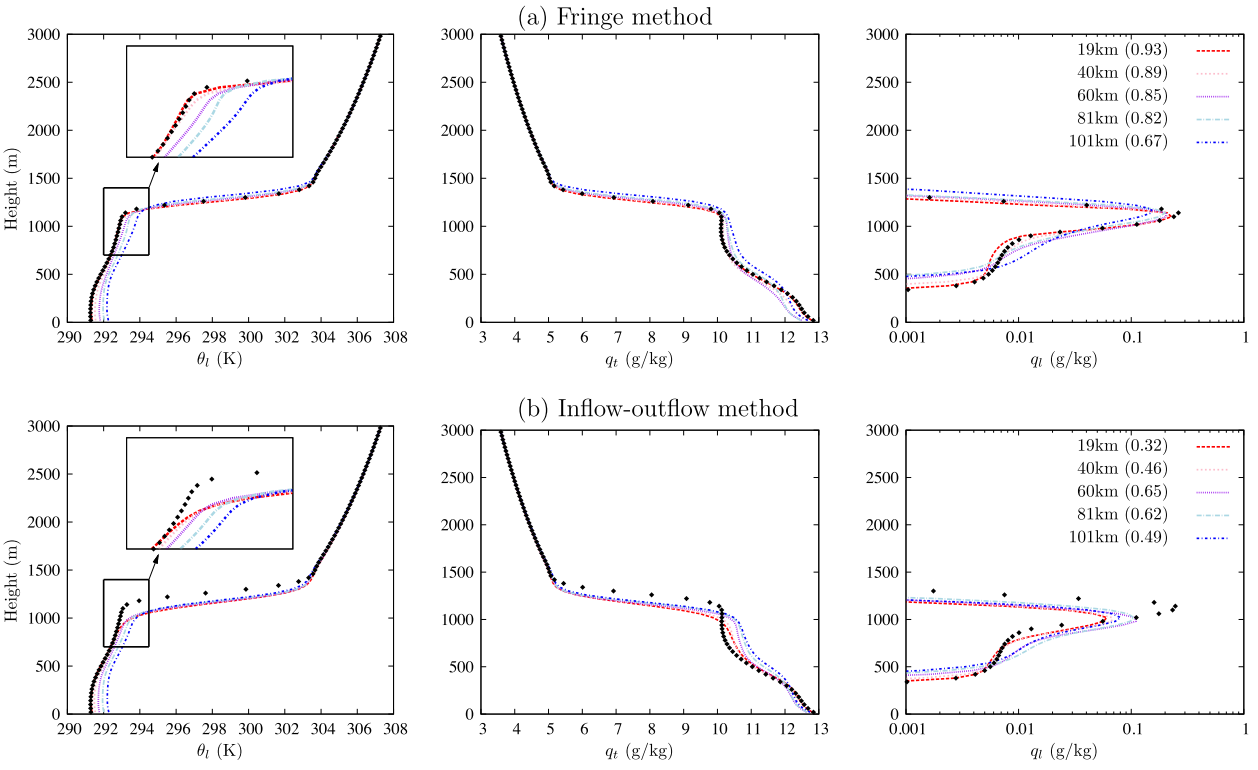

FIG. 4. Vertical profiles of (left) the liquid water potential temperature θ_l, (middle) the total water mixing ratio q_t, and (right) the liquid water mixing ratio q_l: (a) the fringe method and (b) the inflow–outflow method. The black circles show the horizontal average in domain A and the dashed lines show the spanwise averaged data at five different locations from domain B. All data are time averaged over 18 h using data with 10-min interval. Cloud fraction at each location is indicated in the legend.

that the fringe method affects the flow field outside of the fringe region, but the affected area is limited to about 10 km upstream of the fringe region.

Figures 4a and 4b show the vertical profiles of liquid water potential temperature, total water mixing ratio, and liquid water mixing ratio from the fringe and the inflow–outflow method, respectively. Lines are time–spanwise-averaged data at five downstream locations of domain B. Black circles denoting the horizontal-averaged data from domain A are added as a reference. The profiles seem to evolve similarly in both methods, but it is clear that the inversion height decreases in the inflow–outflow method.

To qualitatively evaluate the cloud amount and organization, Fig. 5 shows a snapshot of liquid water path (LWP) that corresponds to the end of the simulations using the fringe method; q_l is integrated spanwise for the side view and in the vertical direction for the top view. A stratocumulus deck on top of cumulus thermals created in domain A enters domain B and evolves and breaks up while being advected along the streamwise direction. The clouds appear to thicken and organize as larger patches as they respond to the increase in surface latent heat flux caused by the SST increase.

5. Conclusions

A new large-eddy simulation (LES) implementation with the fringe approach is described. It is demonstrated that the fringe method provides a better representation than the inflow–outflow method of a spatially developing atmospheric boundary layer (ABL), such as the stratocumulus to shallow cumulus cloud (Sc–Cu) transition. One obvious advantage of the fringe method over the inflow–outflow method is that the periodicity of the flow field is retained and an outflow boundary condition is not required. By simply adding a linear forcing term, the flow inside the fringe region is forced to that of the desired state, which is provided by another concurrently running LES. The fringe method is less affected by artificially reflected waves, which cause unphysical behavior of the ABL such as the decreasing of the boundary layer height as observed in the inflow–outflow method case. The success of the fringe method is attributed to the fact that the fringe region absorbs the horizontally propagating waves at both ends of the domain. Mayor et al. (2002) reported that reflected gravity waves amplify over time and limit the depth of ABL and the duration of the simulation. Enforcing the proper lateral boundary conditions

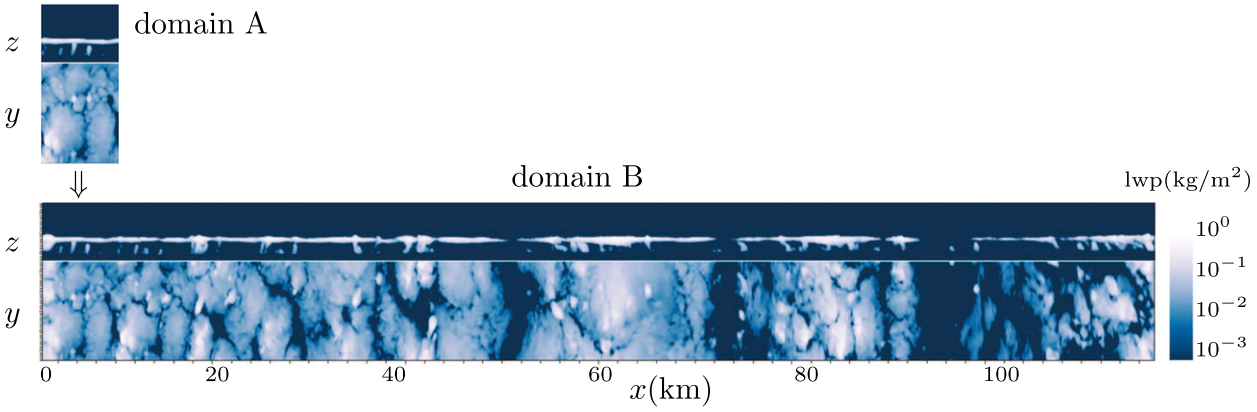

FIG. 5. Visualization of cloudiness for the simulation with the fringe method. The liquid water mixing ratio is integrated spanwise for the side view and in the vertical direction for the top view. The size of domain A and domain B is 7.68 km × 5.12 km × 3.00 km and 115.2 km × 5.12 km × 3.00 km, respectively. The domain size is not to scale; it is enlarged in y, z direction.

is still challenging for some atmospheric simulations. The present results show only the first part of an evolution toward a full Cu transition. Detailed features of the complete Sc–Cu transition structure will be investigated and discussed in a future paper, where results for larger domains and/or different gradients of SST and divergence show a more realistic transition.

Acknowledgments. The authors acknowledge the support provided by the Office of Naval Research, Marine Meteorology Program under Awards N0001411IP20087 and N0001411IP20069, the NASA MAP Program, and the NOAA/CPO MAPP Program. Helpful discussions with K. Suselj and K. Suzuki (JPL) are also greatly acknowledged. This research was carried out at the Jet Propulsion Laboratory, California Institute of Technology, under a contract with the National Aeronautics and Space Administration.

REFERENCES

Bretherton, C. S., S. K. Krueger, M. C. Wyant, P. Bechtold, E. Van Meijgaard, B. Stevens, and J. Teixeira, 1999: A GCSS boundary-layer cloud model intercomparison study of the first ASTEX Lagrangian experiment. *Bound.-Layer Meteor.,* **93,** 341–380, doi:10.1023/A:1002005429969.

Chow, F. K., and R. L. Street, 2009: Evaluation of turbulence closure models for large-eddy simulation over complex terrain: Flow over Askervein Hill. *J. Appl. Meteor. Climatol.,* **48,** 1050–1065, doi:10.1175/2008JAMC1862.1.

Chung, D., and G. Matheou, 2014: Large-eddy simulation of stratified turbulence. Part I: A vortex-based subgrid-scale model. *J. Atmos. Sci.,* **71,** 1863–1879, doi:10.1175/JAS-D-13-0126.1.

——, ——, and J. Teixeira, 2012: Steady-state large-eddy simulations to study the stratocumulus to shallow cumulus cloud transition. *J. Atmos. Sci.,* **69,** 3264–3276, doi:10.1175/JAS-D-11-0256.1.

Colonius, T., 2004: Modeling artificial boundary conditions for compressible flow. *Annu. Rev. Fluid Mech.,* **36,** 315–345, doi:10.1146/annurev.fluid.36.050802.121930.

Cuijpers, J., and P. G. Duynkerke, 1993: Large eddy simulation of trade wind cumulus clouds. *J. Atmos. Sci.,* **50,** 3894–3908, doi:10.1175/1520-0469(1993)050<3894:LESOTW>2.0.CO;2.

Davies, H. C., 1983: Limitations of some common lateral boundary schemes used in regional NWP models. *Mon. Wea. Rev.,* **111,** 1002–1012, doi:10.1175/1520-0493(1983)111<1002:LOSCLB>2.0.CO;2.

De Szoeke, S. P., and C. S. Bretherton, 2004: Quasi-Lagrangian large eddy simulations of cross-equatorial flow in the east Pacific atmospheric boundary layer. *J. Atmos. Sci.,* **61,** 1837–1858, doi:10.1175/1520-0469(2004)061<1837:QLESOC>2.0.CO;2.

Durran, D. R., 1999: *Numerical Methods for Wave Equations in Geophysical Fluid Dynamics.* Springer, 465 pp.

Duynkerke, P. G., and Coauthors, 1999: Intercomparison of three- and one-dimensional model simulations and aircraft observations of stratocumulus. *Bound.-Layer Meteor.,* **92,** 453–487, doi:10.1023/A:1002006919256.

Harlow, F. H., and J. E. Welch, 1965: Numerical calculation of time-dependent viscous incompressible flow of fluid with free surface. *Phys. Fluids,* **8,** 2182, doi:10.1063/1.1761178.

Klemp, J. B., and R. B. Wilhelmson, 1978: The simulation of three-dimensional convective storm dynamics. *J. Atmos. Sci.,* **35,** 1070–1096, doi:10.1175/1520-0469(1978)035<1070:TSOTDC>2.0.CO;2.

Krueger, S. K., G. T. McLean, and Q. Fu, 1995: Numerical simulation of the stratus-to-cumulus transition in the subtropical marine boundary layer. Part I: Boundary-layer structure. *J. Atmos. Sci.,* **52,** 2839–2850, doi:10.1175/1520-0469(1995)052<2839:NSOTST>2.0.CO;2.

Lund, T. S., X. Wu, and K. D. Squires, 1998: Generation of turbulent inflow data for spatially-developing boundary layer simulations. *J. Comput. Phys.,* **140,** 233–258, doi:10.1006/jcph.1998.5882.

Mayor, S. D., P. R. Spalart, and G. J. Tripoli, 2002: Application of a perturbation recycling method in the large-eddy simulation of a mesoscale convective internal boundary layer. *J. Atmos. Sci.,* **59,** 2385–2395, doi:10.1175/1520-0469(2002)059<2385:AOAPRM>2.0.CO;2.

Misra, A., and D. I. Pullin, 1997: A vortex-based subgrid stress model for large-eddy simulation. *Phys. Fluids,* **9,** 2443, doi:10.1063/1.869361.

Nakayama, H., T. Takemi, and H. Nagai, 2012: Large-eddy simulation of urban boundary-layer flows by generating turbulent

inflows from mesoscale meteorological simulations. *Atmos. Sci. Lett.,* **13,** 180–186, doi:10.1002/asl.377.

Nordström, J., N. Nordin, and D. Henningson, 1999: The fringe region technique and the Fourier method used in the direct numerical simulation of spatially evolving viscous flows. *SIAM J. Sci. Comput.,* **20,** 1365–1393, doi:10.1137/S1064827596310251.

Ogura, Y., and N. A. Phillips, 1962: Scale analysis of deep and shallow convection in the atmosphere. *J. Atmos. Sci.,* **19,** 173–179, doi:10.1175/1520-0469(1962)019<0173:SAODAS>2.0.CO;2.

Orlanski, I., 1976: A simple boundary condition for unbounded hyperbolic flows. *J. Comput. Phys.,* **21,** 251–269, doi:10.1016/0021-9991(76)90023-1.

Pullin, D. I., 2000: A vortex-based model for the subgrid flux of a passive scalar. *Phys. Fluids,* **12,** 2311, doi:10.1063/1.1287512.

Samelson, R. M., E. D. Skyllingstad, D. B. Chelton, S. K. Esbensen, L. W. O'Neill, and N. Thum, 2006: On the coupling of wind stress and sea surface temperature. *J. Climate,* **19,** 1557–1566, doi:10.1175/JCLI3682.1.

Sandu, I., and B. Stevens, 2011: On the factors modulating the stratocumulus to cumulus transitions. *J. Atmos. Sci.,* **68,** 1865–1881, doi:10.1175/2011JAS3614.1.

Schlatter, P., S. Stolz, and L. Kleiser, 2006: Large-eddy simulation of spatial transition in plane channel flow. *J. Turbul.,* **7** (33), doi:10.1080/14685240600602929.

Silva Lopes, A., J. M. L. M. Palma, and F. A. Castro, 2007: Simulation of the Askervein flow. Part 2: Large-eddy simulations. *Bound.-Layer Meteor.,* **125,** 85–108, doi:10.1007/s10546-007-9195-4.

Simens, M. P., J. Jiménez, S. Hoyas, and Y. Mizuno, 2009: A high-resolution code for turbulent boundary layers. *J. Comput. Phys.,* **228,** 4218–4231, doi:10.1016/j.jcp.2009.02.031.

Skyllingstad, E. D., D. Vickers, L. Mahrt, and R. Samelson, 2007: Effects of mesoscale sea-surface temperature fronts on the marine atmospheric boundary layer. *Bound.-Layer Meteor.,* **123,** 219–237, doi:10.1007/s10546-006-9127-8.

Spalart, P. R., 1989: Direct numerical study of leading-edge contamination. Fluid dynamics of three-dimensional turbulent shear flows and transition, AGARD-CP-438, Advisory Group for Aerospace Research & Development, 5-1. [Available online at http://www.dtic.mil/dtic/tr/fulltext/u2/a211101.pdf.]

——, and J. H. Watmuff, 1993: Experimental and numerical study of a turbulent boundary layer with pressure gradients. *J. Fluid Mech.,* **249,** 337–371, doi:10.1017/S002211209300120X.

——, R. D. Moser, and M. M. Rogers, 1991: Spectral methods for the Navier-Stokes equations with one infinite and two periodic directions. *J. Comput. Phys.,* **96,** 297–324, doi:10.1016/0021-9991(91)90238-G.

Stevens, B., 2000: Cloud transitions and decoupling in shear-free stratocumulus-topped boundary layers. *Geophys. Res. Lett.,* **27,** 2557–2560, doi:10.1029/1999GL011257.

Voelkl, T., D. I. Pullin, and D. C. Chan, 2000: A physical-space version of the stretched-vortex subgrid-stress model for large-eddy simulation. *Phys. Fluids,* **12,** 1810, doi:10.1063/1.870429.

Wyant, M. C., C. S. Bretherton, H. A. Rand, and D. E. Stevens, 1997: Numerical simulations and a conceptual model of the stratocumulus to trade cumulus transition. *J. Atmos. Sci.,* **54,** 168–192, doi:10.1175/1520-0469(1997)054<0168:NSAACM>2.0.CO;2.